Manipulating Crystal Growth and Polymorphism by Confinement in Nanoscale Crystallization Chambers

BENJAMIN D. HAMILTON,[†] JEONG-MYEONG HA,[†, ‖]
MARC A. HILLMYER,[*, ‡] AND MICHAEL D. WARD[*, §]

[†]Department of Chemical Engineering and Materials Science and, [‡]Department of Chemistry, University of Minnesota, Minneapolis, Minnesota 55455, United States, and [§]Molecular Design Institute, Department of Chemistry, New York University, 100 Washington Square East, New York, New York 10003-6688, United States

CONSPECTUS

The phase behaviors of crystalline solids embedded within nanoporous matrices have been studied for decades. Classic nucleation theory conjectures that phase stability is determined by the balance between an unfavorable surface free energy and a stabilizing volume free energy. The size constraint imposed by nanometer-scale pores during crystallization results in large ratios of surface area to volume, which are reflected in crystal properties. For example, melting points and enthalpies of fusion of nanoscale crystals can differ drastically from their bulk scale counterparts. Moreover, confinement within nanoscale pores can dramatically influence crystallization pathways and crystal polymorphism, particularly when the pore dimensions are comparable to the critical size of an emerging nucleus. At this tipping point, the surface and volume free energies are in delicate balance and polymorph stability rankings may differ from bulk. Recent investigations have demonstrated that confined crystallization can be used to screen for and control polymorphism. In the food, pharmaceutical, explosive, and dye technological sectors, this understanding and control over polymorphism is critical both for function and for regulatory compliance.
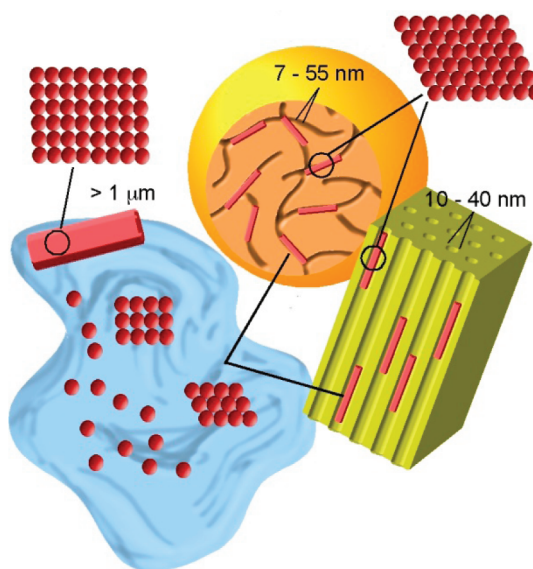
This Account reviews recent studies of the polymorphic and thermotropic properties of crystalline materials embedded in the nanometer-scale pores of porous glass powders and porous block-polymer-derived plastic monoliths. The embedded nanocrystals exhibit an array of phase behaviors, including the selective formation of metastable amorphous and crystalline phases, thermodynamic stabilization of normally metastable phases, size-dependent polymorphism, formation of new polymorphs, and shifts of thermotropic relationships between polymorphs. Size confinement also permits the measurement of thermotropic properties that cannot be measured in bulk materials using conventional methods. Well-aligned cylindrical pores of the polymer monoliths also allow determination and manipulation of nanocrystal orientation. In these systems, the constraints imposed by the pore walls result in a competition between crystal nuclei that favors those with the fastest growth direction aligned with the pore axis.

Collectively, the examples described in this Account provide substantial insight into crystallization at a size scale that is difficult to realize by other means. Moreover, the behaviors resulting from nanoscopic confinement are remarkably consistent for a wide range of compounds, suggesting a reliable approach to studying the phase behaviors of compounds at the nanoscale. Newly emerging classes of porous materials promise expanded explorations of crystal growth under confinement and new routes to controlling crystallization outcomes.

Introduction

The phase behavior of matter embedded in nanoporous matrices has intrigued for decades, largely because the physical constraints on the size of an embedded material enforces large surface-to-volume ratios that are reflected in dramatically different physical properties compared with bulk-scale counterparts. This is most apparent with respect to melting point depression, which becomes more significant with decreasing size. Melting point depression dovetails with classical nucleation theory, which posits that the free energy of a nucleus is determined by the balance between an unfavorable surface energy and stabilizing volume energy. Melting point depression in nanoscale pores also reflects the balance between these two factors, and its existence suggests that the thermodynamic stability of embedded phases and their nucleation, typically regarded as a kinetic effect, are inextricably linked at this length scale. Interestingly, polymorphism, the ability of a compound to adopt multiple crystalline forms, is thought to result from competition between nanometer-scale clusters of molecules that resemble their corresponding mature crystalline forms. Recent investigations have revealed that confined crystallization can be used to screen for, and even control, polymorphism. This can be invaluable to the food, pharmaceutical, explosive, and dye industries, for which regulatory compliance and functional performance depend on polymorph identity and control.

This Account reviews the latest advances in understanding the polymorphic and thermotropic properties of crystalline materials embedded in the nanometer-scale pores of porous glass powders and polymer monoliths, the latter generated by selective etching of one polymer block component from a shear-aligned diblock or triblock polymer monolith. Compounds embedded in these materials exhibit an assortment of size-dependent phase behaviors, including the selective formation and stabilization of metastable amorphous and crystalline phases, the shift of thermotropic relationships (i.e., monotropic vs enantiotropic) among polymorphs, and the discovery of previously unknown polymorphs. Size confinement also permits determination of polymorph thermotropic properties that are impossible to measure in bulk forms. Furthermore, macroscopic polymer monoliths and other matrices with highly aligned cylindrical pores enable the examination of nanocrystal orientation under confinement, with preferred orientations resulting from a competition between crystal nuclei whose sizes are unconstrained only in one dimension. This phenomenon provides an opportunity to examine the influence of tailored additives, which bind to specific crystal faces, on growth rate and orientation of embedded crystals at a length scale not achievable by any other means. We conclude with a look at likely future directions for this area.

Nucleation: Classical Models

The initial stage of crystal growth is typically described as a small cluster of molecules (aka, a nucleus), the formation of which is accompanied by a free energy change, ΔG^{cryst} (Figure 1A), which is the sum of the negative (favorable) volume free energy change, ΔG_V, which scales with the interatomic (or intermolecular) bonding energy, and the positive (unfavorable) surface free energy change, ΔG_A, associated with the phase boundary between the emerging nucleus and the surrounding medium. ΔG^{cryst} is size-dependent, exhibiting a maximum that defines the activation energy for nucleation, ΔG_{crit}, and the "critical radius," r_{crit}. Nuclei smaller than r_{crit} spontaneously dissolve whereas nuclei larger than r_{crit} spontaneously grow. Critical sizes are typically regarded as nanometer scale.[1] When compounds can adopt multiple polymorphs, the energetic profiles of the competing crystal forms determine the crystallization outcome (Figure 1B). These profiles, and thus the stability ranking of emerging polymorphs at the critical length scale, can be adjusted by manipulating the environment through conventional process variables such as solvent[2] and temperature.[3] Moreover, additives can stabilize or arrest the growth of a particular form.[4] Recognizing that nucleation almost always occurs on surfaces, well-defined solid substrates and monolayers at the air−water interface have been employed to regulate nucleation.[5,6] The features of the free energy curves in Figure 1B argue that polymorphism also can be controlled by intervening in the crystallization process at the nanometer scale, in the vicinity of the critical size, at which the polymorph nuclei will differ with respect to their thermodynamic stability. The use of nanoporous matrices as crystallization reactors in which the pores serve to confine crystallization at length scales along the trajectory of Figure 1B provides an opportunity to explore this phenomenon and enable control of polymorphism and polymorph screening, particularly if the pore sizes are adjustable.

The influence of crystal size on melting temperature becomes apparent at the nanoscale, where it has been described by the Gibbs−Thomson equation (eq 1),[7] where M is the molecular mass of the compound comprising the particle, ρ is the particle density, r is the particle radius
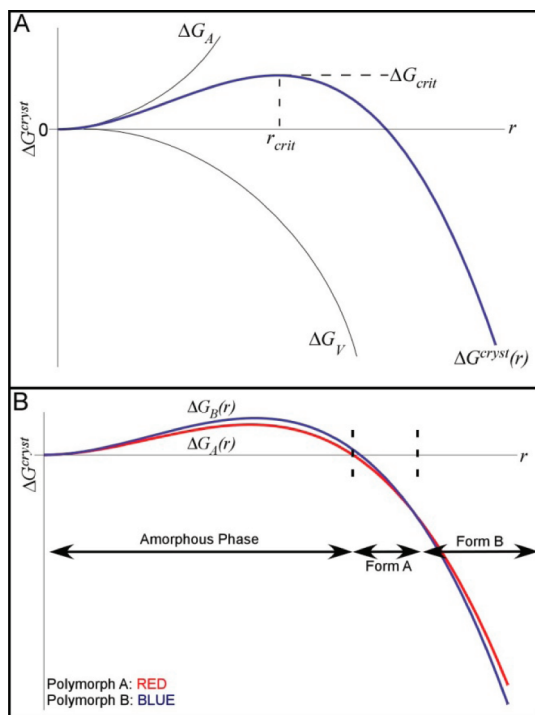
FIGURE 1. (A) Illustration of the free energy (ΔG^{cryst}) profile of a growing crystal nucleus as a function of crystal radius, r. The energy profile results from the sum of the favorable volume free energy, ΔG_V, and the surface free energy penalty associated with forming an interface between the original and new phases, ΔG_A. The profile passes through a maximum value of ΔG_{crit} at r_{crit}. (B) Illustration of the energetic profiles for two competing nuclei, polymorph A and polymorph B, over a range of characteristic lengths. The thermodynamically preferred phase corresponds to the lowest free energy, which can be adjusted by placing nanometer size constraints upon the growing nuclei. Kinetics and thermodynamics intersect at the critical size; at the critical size, the difference in the kinetic barrier for the two polymorphs is tantamount to the difference in their thermodynamic stability at this size. This ranking can persist beyond the critical size but reverse to the stability ranking of the bulk as the size increases.

(assuming spherical shape), γ_{nl} is the surface tension (interfacial energy) between the condensed phase and the fluid surrounding it, θ is the interfacial angle between the condensed phase and a contacting surface, ΔH^{fus} is the molar heat of fusion of the bulk condensed phase, $T_m(r)$ is the melting temperature of the condensed phase of radius r, and $T_{m,bulk}$ is the melting temperature of the condensed phase in the bulk (as $r \rightarrow \infty$).

$$\frac{T_{m,bulk} - T_m(r)}{T_{m,bulk}} = -\frac{2M}{\Delta H^{fus}\rho r}\gamma_{nl}\cos\theta \qquad (1)$$

$$\frac{T_{m,bulk} - T_m(r)}{T_{m,bulk}} = \frac{2M}{\Delta H^{fus}\rho r}\gamma_{nl} \qquad (2)$$

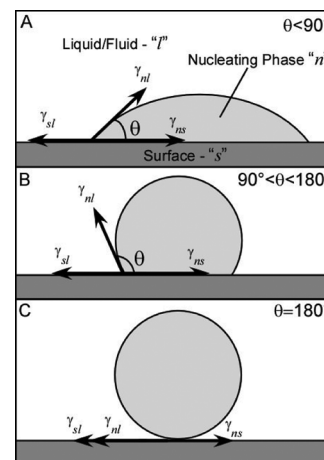The Gibbs−Thomson equation predicts a linear relationship between the change in melting point, $T_{m,bulk} - T_m(r)$,

FIGURE 2. Illustration of the static equilibrium described by the Young equation. Three interfacial tensions, γ_{sl}, γ_{ns}, and γ_{nl} are balanced at a contact angle θ between the nucleating phase and the surface. (A) Favorable nucleus−surface interactions, that is, good wetting, results in $\theta < 90°$. (B) Unfavorable nucleus−surface interactions (poor wetting) results in $90° < \theta < 180°$. (C) A complete absence of wetting results in $\theta = 180°$, which is the customary assumption for applications of the Gibbs−Thomson equation.

and the inverse particle size, $1/r$, assuming the other parameters are independent of size. The θ term in eq 1 is generally assumed to be 180°, which is valid for homogeneous nuclei that do not wet the aforementioned surface. This assumption is pervasive in the literature, to the extent that the $\cos\theta$ term often is ignored in favor of a simplified form (eq 2), even in cases for which wetting ($\theta < 90°$) is expected. The Gibbs−Thomson equation also can be combined with the Young equation (eq 3) to generate a form that encompasses the dependence of the melting point on the interfacial energies between the particle (n), surrounding fluid (l), and substrate (s) (Figure 2, eq 4). We recently invoked this form to explain melting point behaviors that deviated from those expected based on the (erroneous) assumption that $\theta = 180°$.[8]

$$\gamma_{ns} - \gamma_{sl} = \gamma_{nl}\cos\theta \qquad (3)$$

$$\frac{T_{m,bulk} - T_m(r)}{T_{m,bulk}} = \frac{2M(\gamma_{ns} - \gamma_{sl})}{\Delta H^{fus}\rho r} \qquad (4)$$

There are a number of assumptions implicit in classical nucleation and the Gibbs−Thomson equation that can produce discrepancies between predicted and observed behaviors. Some of these have been addressed in a recent Account[9] describing the current understanding of nucleation theory. A portion of the Account herein addresses other physical properties often assumed (incorrectly) to be unimportant, independent of size, or constant, namely γ, ΔH^{fus},

and ρ. Notably, no analytic treatments analogous to the Gibbs–Thomson equation exist that describe the dependence of solid-state transformations, such as amorphous-to-crystalline or polymorph transitions, on crystal size. In part, this is because nonmelting transitions such as freezing, vitrification, and solid-state phase transitions are subject to ill-defined kinetic factors such as defects, impurities, molecular diffusion, and conformational rearrangements, any of which may contribute to the rate of transformation.

Thermotropic Properties of Ultrasmall Crystals in Nanoporous Silaceous Matrices

Christenson[10] and Alcoutlabi and McKenna[11] have described the history of the dependence of glass transition temperatures and melting temperatures on size confinement. Most previous descriptions of melting behavior adhere to the linear relationship expected between ΔT_m and $1/r$ described by the Gibbs–Thomson equation (eq 1), despite reports of the size dependence of ΔH^{fus}, which should produce a nonlinear relationship between ΔT_m and $1/r$. A disordered liquid layer surrounding the crystal was suggested to be responsible for the reduction of ΔH^{fus},[11,13] noting that nuclei of various sizes surrounded by a shell of amorphous material with a fixed thickness would be more liquid-like for smaller nuclei, where the surface-to-volume ratio becomes significant. Certain compounds, such as benzene and carbon tetrachloride, exhibited melting point depressions and elevations, the extent of which depended on the composition of the porous matrix. These reports, however, do not address the $\theta = 180°$ assumption often invoked for the Gibbs–Thomson equation, despite the clear dependence of ΔT_m on the porous matrix composition.

Rault et al.[12] reported thicknesses of noncrystallizing layers ranging from ∼0.6 to 1.5 nm thick, invoking a combined crystal and amorphous layer with thicknesses between ∼1.5 and ∼3 nm, below which no crystallization occurred. This thickness may reflect a critical size for nucleation. Jackson and McKenna[13] also examined the effect of decreasing pore size on the crystallization and vitrification of *o*-terphenyl and benzyl alcohol within CPG powders. Their results revealed that crystallization of amorphous phases could be suppressed in pores with diameters both less than and greater than $2r_{crit}$, which was estimated by substituting bulk-scale values for physical parameters into a modified form of the Gibbs–Thomson equation, implicating both *kinetic stabilization of the amorphous phase in pores large enough to accommodate postcritical nuclei* and *thermodynamic stabilization of the amorphous phase in pores too small to support stable crystals.*
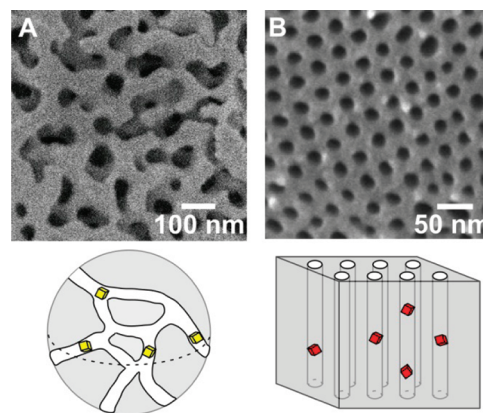

FIGURE 3. (Top) Scanning electron micrographs of (A) commercially available controlled pore glass (CPG) with a pore diameter, $d \approx 55$ nm. (B) A platinum-coated (ca. 2 nm thick) p-PCHE monolith with a hexagonal array of cylindrical pores ($d \approx 30$ nm). (Bottom) Schematic representations of nanocrystals grown in the pores of each type of porous matrix. Whereas the pores in CPG are random, the cylindrical pores in p-PCHE are highly ordered, permitting examination of crystal orientation with respect to the pore direction. The refractory nature of CPG permits infiltration of the melts of compounds with melting points higher than T_g of the nanoporous polymer monoliths, above which the polymer softens and the pores collapse. The refractory nature of CPG also permits characterization of the thermotropic properties of embedded crystals at higher temperatures. Reproduced from ref 26. Copyright 2009 American Chemical Society.

New Explorations Using Engineered Nanoporous Matrices

Porous matrices such as Vycor and controlled pore glass (CPG) permit systematic measurements of the key parameters in the Gibbs–Thomson equation. These materials, however, contain random and tortuous pores with broad pore size distributions (Figure 3A) within the same matrix. Moreover, junctions created by intersecting pores could be expected to have larger volumes locally. Recently, we developed macroscopic polymeric matrices with highly ordered cylindrical nanopores and very narrow size distributions. These nanoporous monoliths were created by shear alignment of block polymers consisting of two (or more) immiscible segments that can form a self-assembled structure consisting of nanometer-scale cylindrical domains embedded in a chemically distinct matrix.[14] After shear alignment, chemical etching of the cylindrical block affords macroscopic monoliths with highly ordered, continuous cylindrical nanopores aligned along a single direction of the monolith (Figure 3B). These nanoporous monoliths have been generated from polystyrene–polylactide[15] (PS–PLA) and poly(cyclohexylethylene)–polylactide (PCHE–PLA)[16] diblock polymers, as well as polystyrene–poly(dimethylacrylamide)–polylactide (PS–PDMA–PLA) triblocks.[17] In each case, the PLA
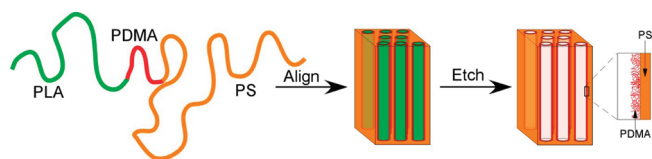
FIGURE 4. Schematic representation of the fabrication of nanoporous polymer monoliths from a block polymer. Triblock terpolymers consisting of polylactide (PLA), poly(dimethylacrylamide) (PDMA), and polystyrene (PS) are shear-aligned to form a PS matrix and hexagonally ordered cylinders of PLA surrounded by a shell of PDMA. Etching of the PLA component produces cylindrical pores lined with hydrophilic PDMA. Adapted from ref 17b.

component that forms the cylinders is chemically etched under mild conditions. The pores generated from etching PS–PLA and PCHE–PLA are hydrophobic, whereas removal of the PLA block from PS–PDMA–PLA produces hydrophilic PDMA-coated pore walls (Figure 4). Pore sizes can be regulated by adjustment of the volume fraction of each block and the overall molecular weight, with pore sizes practically achievable in the range $10 < d < 100$ nm. The ability to regulate pore size and pore wall composition in these nonsiliceous nanoporous matrices, coupled with narrow size distributions and high degree of alignment, expands the range of phenomena that can be probed for embedded materials.

Polymorphism and Thermotropic Properties of Nanocrystals

In 2004, Ha et al.[18] crystallized anthranilic acid (AA), for which three polymorphs are known, within CPG having pores with average diameters of 7.5, 24 and 55 nm. Form III crystallized in 55 nm CPG and on the surfaces of nonporous glass beads, a mixture of forms II and III were observed in 24 nm CPG, and only form II was observed in 7.5 nm CPG. Form III is the thermodynamically stable phase in the bulk, but form II persisted in the pores indefinitely. The exclusion of form III in 7.5 nm CPG was attributed to its larger critical nucleus size. Moreover, the persistence of form II may reflect a lower free energy compared with the other forms at or slightly beyond the critical size (Figure 1B), reflecting *size-dependent polymorph stability*. This report also described the crystallization of 5-methyl-2-[(2-nitrophenyl)-amino]-3-thiophenecarbonitrile, known as ROY for the red, orange, and yellow colors of its polymorphs,[19] within the 20 and 30 nm cylindrical pores of nanoporous PCHE monoliths. Within 30 nm PCHE monoliths, ROY crystallized as the Y form (corresponding to yellow prisms) upon evaporation of solvent (pyridine) used to carry ROY into the pores. When the PCHE monolith containing the embedded crystals was
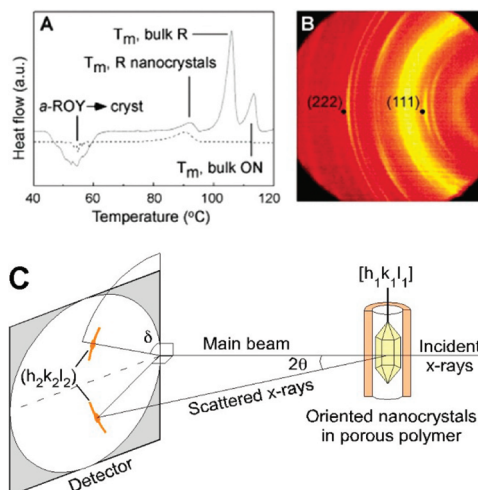

FIGURE 5. (A) DSC of an unwashed (solid line) and washed (dashed line) nanoporous PCHE monolith impregnated with ROY (from pyridine solvent) that has been subjected to heating at 120 °C and cooled to −25 °C (5 °C/min in both directions). (B) Two-dimensional diffraction pattern of an aligned monolith containing only R nanocrystals. Preferred orientation of R nanocrystals is evident in the azimuthal intensity maxima exhibited by the reflections. For clarity, only the (111) and (222) reflections are denoted here. Reproduced from rom ref 18. Copyright 2004 American Chemical Society. (C) Configuration for diffraction using μ-XRD. The nanoporous monolith with embedded nanocrystals (depicted here as only a single cylinder) is held in a fixed orientation with respect to a 2D detector. Reflections from specific crystal planes produce diffraction features at coordinates $(2\theta,\delta)$, where 2θ is the Bragg diffraction angle and δ corresponds to the orientation of that plane with respect to $\delta = 0$, which coincides here with the pore axis. Arcs of intensity (rather than discrete points) signify a distribution of orientations of the reflecting plane about the preferred orientation, and the breadth of the arcs can be used to measure the alignment distribution within the pores. Adapted from ref 31. Copyright 2009 American Chemical Society.

heated above the melting temperature of ROY and then cooled, the embedded melt recrystallized as the aligned R form with the (111) crystal planes parallel to the pore direction, as determined by X-ray microdiffraction (Figure 5). Interestingly, crystallization of Y and R was suppressed in the PCHE monoliths with 20 nm pores in favor of the red amorphous phase, *a*-ROY. This behavior was attributed to amorphous phase stabilization resulting from the small pore dimensions constraining particle size to a value below r_{crit} for ROY.

Ha et al. also reported the melting behaviors of *R*-methyl adipic acid (RMAA) and 2,2,3,3,4,4-hexafluoropentane-1,6-diol (HFPD) in CPG and porous PS monoliths.[8] The melting temperature dependence on pore size adhered to the $1/r$ dependence of the Gibbs–Thomson equation (eq 1). The slope of ΔT_m vs $1/r$ differed for HFPD embedded in CPG and p-PS (Figure 6), suggesting a dependence on the porous matrix, that is, $\theta \neq 180°$. This behavior was regarded as evidence that the θ term cannot be ignored and that the "full" Gibbs–Thompson
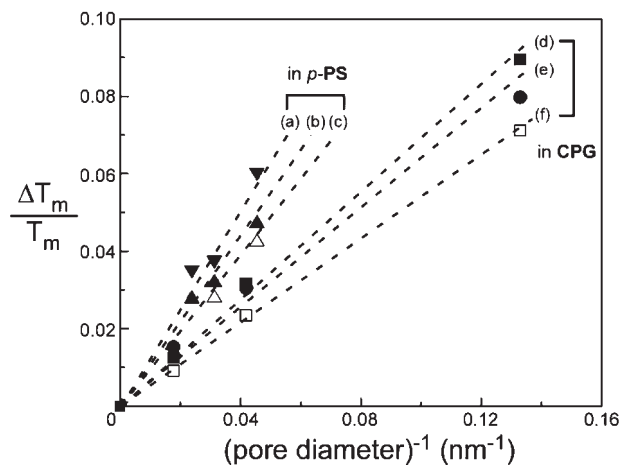
FIGURE 6. Dependence of the normalized melting point depression, $\Delta T_m/T_m$, on the channel diameter for (a, ▼) R-MAA in p-PS, imbibed from methanol, (b, ▲) HFPD in p-PS, (c, △) HFPD in p-PS, imbibed from melt, (d, ●) HFPD in CPG, imbibed from methanol, (e, ●) R-MAA in CPG, imbibed from methanol, and (f, □) HFPD in CPG imbibed from melt. The slopes are larger for the p-PS monoliths. The data for HFPD reveal that the effect of the porous matrix outweighs the differences arising from the method used to introduce the HFPD to the channels (melt or methanol solutions). The dashed lines represent the best fit to each data set, including a point added at $\Delta T_m/T_m = 0$, $1/d = 0$, which corresponds to the bulk melting temperature. Reproduced from ref 8. Copyright 2005 American Chemical Society.

equation (eq 1) is more appropriate than the simplified version (eq 2). Surprisingly, the melting point depression exhibited a linear dependence on $1/r$ despite the observation that ΔH^{fus} *also decreased linearly* with increasing $1/r$. Decreasing values of ΔH^{fus} with crystal size were also noted by Alcoutlabi and McKenna.[11] Ha et al.[8] argued that the linearity was due to a fortuitous compensation of the decrease in ΔH^{fus} by a decrease in γ_{nl} with decreasing crystal size because the specific surface energy of the crystal is expected to approach that of a liquid with decreasing crystal size.

A series of manuscripts in 2007 and 2008 reported that acetaminophen, a pharmaceutically relevant compound with three polymorphs, exhibited melting point depression in the pores of CPG and anodic aluminum oxide templates that was consistent with the Gibbs–Thomson equation.[20–22] As with the polymer monoliths described above, the CPG monoliths afford easy handling and cleaning. The refractory nature of CPG, however, permits infiltration of the melts of compounds with melting points higher than T_g of the polymer monoliths, above which the polymer softens and the pores collapse. Within the smallest pore sizes examined, 4.6 nm diameter, crystallization was suppressed in favor of an amorphous phase. The authors suggest that this was due to either *critical size effects* or *a kinetic stabilization of the amorphous phase*, and

note that determining the cause is precluded by challenges in determining whether amorphous acetaminophen is the equilibrium phase in the 4.6 nm pores. In the case of 22−60 nm pores, the metastable form III of acetaminophen was present exclusively. Mixtures of forms II and III formed within 103 nm CPG. The authors posited that the shift from metastable form III in pores less than 60 nm to the more stable form II in pores greater than 100 nm reflected Ostwald's rule of stages. They also noted that upon heating, form III exhibited melting point depression sufficient to induce melting prior to the form III to II transition observed in the bulk. Extrapolation of the Gibbs–Thomson equation to bulk sizes permitted an estimation of the bulk form III melting temperature, which had not been measured directly. The authors also suppressed the crystallization of these forms by rapidly quenching molten acetaminophen, resulting in an amorphous phase that recrystallized slowly over time. The glass transition temperature decreased with decreasing pore size and broadened significantly for 4.6 nm CPG. The authors attributed the broadening to strong interactions between acetaminophen layers and pore walls, which immobilized the outermost acetominophen layers. A size-dependent T_m broadening was attributed to a growing influence of a noncrystallized layer, which would exert a negligible effect on melting point properties for larger crystals but would increasingly contribute to the melting behavior of embedded crystals as the crystal size is reduced. The authors suggested that a combination of pore size, crystal–pore wall interactions, and pore topology could be tailored for specific applications, such as the stabilization of pharmaceutical compounds. The same authors noted that CPG could be used to study the effect of nanoscale confinement on the crystallization of polymers.[23]

As described by Hamilton et al. in 2008, glycine, which exhibits three polymorphs in the bulk, was imbibed as an aqueous solution by CPG powders and hydrophilic nanoporous PS–PDMA monoliths (Figure 7).[24] Crystallization in both nanoporous matrices exclusively produced β-glycine, the metastable form in the bulk, upon water evaporation. The β-glycine crystals were stable indefinitely when confined within pores having dimensions 24 nm or less, but they slowly transformed to α-glycine, the polymorph typically observed in benchtop crystallizations from aqueous solvent, in 55 nm pores. Extrapolation of plots of size-dependent T_m vs $1/r$ to bulk length scales (i.e., $1/r = 0$) provided an estimate of the bulk β-glycine T_m value, which cannot be measured due to its instability with respect to the α-form and the decomposition of glycine prior to melting. The exclusive presence of β-glycine in the smaller nanopores and the appearance of α-glycine as the
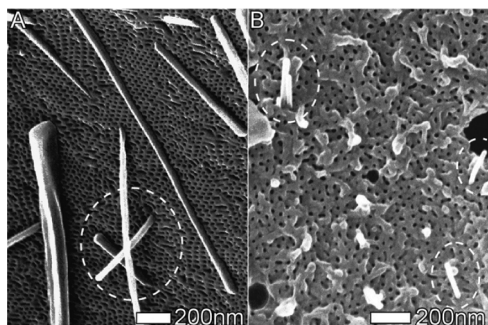
FIGURE 7. SEM images of β-glycine nanocrystals protruding from the pores of a PS–PDMA monolith after evaporation of an aqueous glycine solution containing (A) 18% glycine (w/w water) and (B) 18% glycine and 1.2% (w/w water) *R,S*-phenylalanine auxiliary prior to swabbing. The circled region in panel A highlights glycine nanocrystals protruding from the monolith pores. Reproduced from ref 24. Copyright 2008 American Chemical Society.
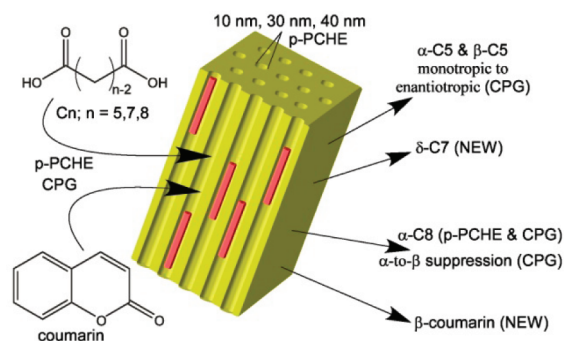

FIGURE 8. Schematic highlighting the results of the crystallization of α,ω-dicarboxylic acids pimelic acid ($n = 7$), glutaric acid ($n = 5$), and suberic acid ($n = 8$), and coumarin in the pores of PCHE and CPG. These crystallizations resulted in the identification of three previously unreported polymorphs. Reproduced from ref 26. Copyright 2009 American Chemical Society.

pore size is increased suggests that the initial stage of glycine crystallization involves formation of β nuclei, followed by their transformation to α-glycine as crystal size increases, in accord with Ostwald's rule of stages.[25]

A 2009 report by Ha et al. detailed the crystallization of pimelic acid, $HO_2C(CH_2)_{n-2}CO_2H$ ($n = 7$), glutaric acid ($n = 5$), suberic acid ($n = 8$), and coumarin (1,2-benzopyrone) in nanometer-scale pores of CPG and PCHE monoliths (Figure 8). Pimelic acid, suberic acid, and coumarin *exhibited previously unknown polymorphs*, denoted δ-pimelic acid, β-suberic acid, and β-coumarin, in CPG with pore sizes <23 nm and p-PCHE with pore diameters <40 nm. The melting points of the confined crystals decreased monotonically with decreasing pore size, in accordance with the Gibbs–Thomson equation. Moreover, the authors reported that the *enantiotropic phase behavior of bulk glutaric acid and suberic acid*

switches to monotropic when those compounds are confined within the nanoscale pores of CPG and p-PCHE.[26] These observations reveal that nanoscale confinement can alter crystallization outcomes and affect polymorph stability compared with bulk crystallization. Moreover, crystallization in very small pores can lead to *the discovery of new polymorphs* that otherwise would not be detected using conventional screening methods.

Nanocrystal Orientation

Nanoporous matrices equipped with well-ordered and highly aligned pores provide a unique opportunity to examine the orientations of the nanocrystals within the pores. For example, ROY embedded in p-PCHE monoliths revealed that the ROY nanocrystals were preferentially aligned with their (111) crystal planes parallel to the pore direction.[17] Nanocrystals of flufenamic acid, α,ω-alkanedicarboxylic acids ($HO_2C(CH_2)_{n-2}CO_2H$, $n = 3-13$, odd) and coumarin also exhibited preferred orientations in p-PCHE monoliths.[27] Henschel et al.[28] recently reported that n-hexane crystals embedded in 10-nm pores of a porous silicon sample adopted orientations consistent with the fast-growth direction of bulk n-hexane crystals aligned parallel to the pore direction. Nanocrystals of larger molecules ($C_nH_{2n+1}OH$, $n = 16, 17, 19$; C_nH_{2n+2}, $n = 16, 17, 19, 25$) adopted orientations in the porous silicon with the alkyl backbones of the molecules aligned perpendicular to the channel direction, consistent with increased dispersive interactions between the longer chains prompting faster growth perpendicular to the chains.[29] Other reports describing the orientation behavior of confined nanocrystals are largely focused on crystalline polymers, as exemplified by poly(vinylidene difluoride) crystals embedded in nanoporous alumina ($\sim$20 nm pore diameter), which tend to grow with their fast-growth direction aligned parallel to the pores.[30]

We recently reported that β-glycine nanocrystals grown in the pores of PS–PDMA were oriented with the [010] axis, the natural fast-growth direction, aligned parallel with the pore direction (the [010] direction is equivalent to the *b*-axis in the monoclinic symmetry of β-glycine).[31] The preferred orientation was regarded as evidence against the instantaneous formation of randomly oriented nuclei that retain their initial orientation and grow uniformly. Instead, the behavior was attributed to a continuous and reversible nucleation and growth process wherein nanoscale nuclei with the fast-growth direction parallel (or nearly parallel) to the pores are preferred because they can surpass a critical length, and therefore a critical volume, more readily than nuclei aligned along a direction in which the fast growth
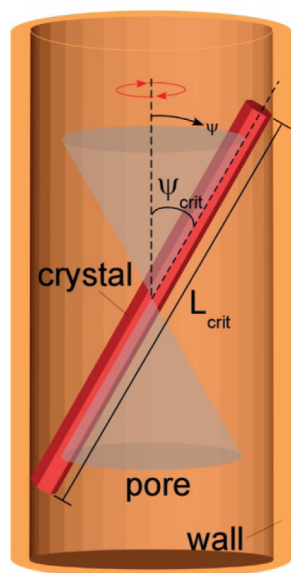
FIGURE 9. Illustration of the geometry of a crystal embedded in a single pore of a nanoporous monolith. The crystal is depicted as tilted by an angle ψ relative to the pore direction without constraint on its rotational orientation about the pore axis. The crystal length will be increasingly constrained for increasing values of ψ, eventually reaching a limit at an angle ψ_{crit}, beyond which the crystal cannot achieve a critical length, L_{crit} *and consequently, a critical volume.* Crystals with $\psi > \psi_{crit}$ are thus inclined to redissolve because they are below the critical size. This behavior leads to a competition between nuclei as they attempt to reach critical sizes, and only nuclei oriented in such a way that they can grow and surpass critical sizes persist. The preferred nanocrystal orientation observed for crystals embedded in highly ordered pores is only one example of how these critical size effects are revealed.

direction would be obstructed by the pore walls (Figure 9). These factors set the stage for a Darwinistic competition wherein crystals with the fast-growth axis aligned with the pores survive while others perish. The behavior of β-glycine is especially interesting because it is chiral and therefore exists as two enantiomorphs ($P2_1$ space group). The crystals have a needle-like habit with one end tapered nearly to a point, indicative of vanishingly small (010) and (0$\overline{1}$0) faces at the crystal tips of the two enantiomorphs, assigned as (010) of the ($+$)-β enantiomorph and (0$\overline{1}$0) of the ($-$)-β enantiomorph. Inspection of the crystal structure of β-glycine leads to the conclusion that these faces have high surface energies. Consequently, the observed crystal alignment, in which these planes are perpendicular to the pore axis, serves to minimize their area and overall surface energy of the nanocrystals as well. Any tilt of this face relative to the pore axis would allow expansion of the surface area of these high-energy planes, thereby increasing the total free energy and prompting dissolution.

Interestingly, racemic mixtures of chiral auxiliaries (*R,S*-phenylalanine, *R,S*-methionine, *R,S*-tryptophan) are known to
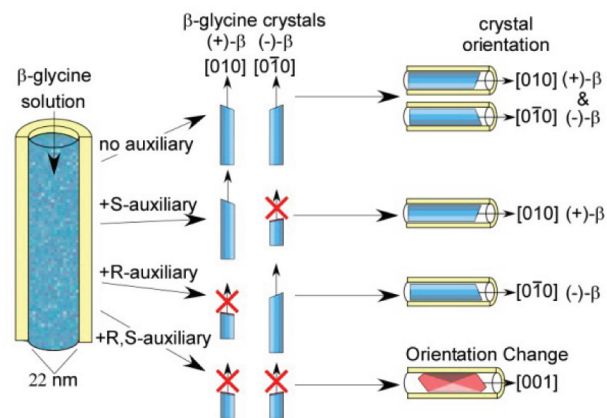

FIGURE 10. Preferred orientations adopted by β-glycine nanocrystals grown within nanoporous PS–PDMA in the absence of chiral auxiliaries or in the presence of enantiopure or racemic mixtures of the auxiliaries. Adapted from ref 31. Copyright 2009 American Chemical Society.

block growth of β-glycine along its fast-growth b axis because of enantioselective binding to the (010) ($+$)-β and (0$\overline{1}$0) ($-$)-β faces (which are perpendicular to the b axis).[32] In the bulk, this binding results in a change of crystal habit from needles to plates with large {010} faces, such that longest crystal dimension is contained within the {010} plane. When crystallization is conducted within the PS–PDMA nanopores in the presence of *racemic* mixtures of these auxiliaries, the β-glycine crystals were oriented with their b axis *perpendicular* to the cylinder axis, that is, rotated 90° compared with the orientation observed in the absence of the auxiliaries (Figure 10)! In contrast, when β-glycine was crystallized in the nanopores in the presence of an *enantiopure* auxiliary, the crystal orientation was identical to that observed in the absence of the auxiliaries. This observation revealed a highly specific recognition of a chiral auxiliary to only one of the enantiomorphs; an enantiopure chiral auxiliary will bind selectively to either (010) of ($+$)-β or (0$\overline{1}$0) of ($-$)-β, depending on the handedness of the auxiliary. Under these conditions, the enantiopure auxiliary will inhibit the growth of only one of the enantiomorphs, allowing the unaffected enantiomorph to grow unimpeded with the [010] axis parallel with the pore direction. This also revealed that specific binding is operative at a length scale comparable to that at which critical nuclei are formed, illustrating that tailored growth inhibitors can influence crystallization outcomes through intervention at the earliest stages of crystallization. Collectively, the observations for β-glycine and the other examples mentioned above corroborate the role of critical size effects, surface energies, and the competition between nuclei, wherein confinement favors growth orientations that permit nuclei to achieve critical size more competitively when their

fast-growth axis is unimpeded by pore walls, regardless of the actual crystal plane normal to that axis (Figure 9).

Outlook

The observations described in this Account represent a remarkable assortment of polymorphic and thermotropic behaviors that become evident when solids are confined to nanopores. The regulation of polymorphism is an issue of critical importance in many technologies, as underscored by challenges in the pharmaceutical sector, where polymorph screening and control are crucial aspects of drug development. The collection of work described herein illustrates polymorph selectivity, phase stabilization, polymorph stability crossovers, suppression of crystalline phases in favor of amorphous phases, and shifts from enantiotropic to monotropic behavior. These observations of size-dependent polymorphism argue that caution must be exercised when devising nanocrystal formulations that are subject to regulations that require polymorph identification and characterization. Moreover, growth in the nanoscale pores affords polymorphs that were previously unreported, suggesting a unique route to polymorph discovery. The subtle dependence of Gibbs—Thomson behavior on the composition of pore walls may offer a new way to manipulate polymorphism and thermotropic properties for confined compounds. Furthermore, the dependence of both melting temperature and glass transition on pore size may permit the study of those properties in confinement as a new method to examine the behaviors of glasses and crystals near the Kauzmann[33] temperature, T_K, the temperature at which the extrapolations of the glass and crystal entropy profiles intersect. The intersection of the extrapolations suggests a paradox where the expected entropy of the glass becomes negative at very low temperatures and thus violates the third law of thermodynamics.[30] Kauzmann's paradox is believed to be avoided by a thermodynamically mandated glass transition,[34] but bulk-scale experiments frequently struggle to decouple the kinetically controlled glass transitions from the thermodynamic ones.

While nanoporous glass matrices are quite useful in studying confined crystallization phenomena, the advent of monolithic nanoporous polymers with well-aligned cylindrical pores, controlled pore wall chemistries, and tunable pore dimensions has opened new doors. In particular, these new materials have enabled investigations of nanocrystal orientation during confined growth. For example, the observations of preferred orientations argue against heterogeneous nucleation wherein a particular crystal plane interacts favorably with the pore walls. Instead, it appears that preferred orientation is a consequence of critical size effects and surface energy considerations, wherein confinement favors growth orientations that permit nuclei to achieve critical size more competitively. The ability to manipulate the orientation of nanocrystals under extreme size confinement may provide new routes to composite materials while enabling exploration of the structure—property relationships at the nanoscale, for example, solid-state reactions occurring in organic nanocrystals with dimensions smaller than those reported previously.[35,36] It is also interesting to consider whether the formation of a noncentrosymmetric crystalline phase because of nanoconfinement, in this case β-glycine, the simplest amino acid, suggests a role for this phenomenon in the genesis or amplification of biological homochirality in clay or mineral matrices.[37]

BIOGRAPHICAL INFORMATION

Benjamin D. Hamilton received a B.S. in Chemical Engineering at Purdue University in 2004 and a Ph.D. at the University of Minnesota in 2009 under the direction of Marc Hillmyer and Michael D. Ward. Hamilton is currently a postdoctoral research associate with Daniel Shantz at Texas A&M's Artie McFerrin Department of Chemical Engineering, where his research interests have centered on the creation of organic-functionalized ceramic hybrid membranes for light gas and liquid separations.

Jeong-Myeong Ha received a B.S. in Chemical Engineering at Seoul National University in 1999 and a Ph.D. at the University of Minnesota in 2006 under the direction of Michael D. Ward. After a postdoctoral research position at the University of California at Berkeley with Alexander Katz, Ha moved to the Korea Institute of Science and Technology (KIST) in Seoul, South Korea, where he is currently a senior research scientist investigating tailor-made nanostructured catalysts for biofuel production and artificial photosynthesis.

Marc A. Hillmyer received a B.S. in Chemistry from the University of Florida in 1989 and a Ph.D. in Chemistry from the California Institute of Technology in 1994. After a postdoctoral position in the University of Minnesota's Department of Chemical Engineering and Materials Science, he joined the Chemistry faculty at Minnesota in 1997. He is currently a Distinguished McKnight University Professor of Chemistry and leads a research group focused on the synthesis and self-assembly of multifunctional polymers. Hillmyer also is an Associate Editor for the ACS journal *Macromolecules* and the director of the University of Minnesota Center for Sustainable Polymer, supported by the National Science Foundation.

Michael D. Ward received a B.S. in Chemistry from the William Paterson College of New Jersey in 1977 and a Ph.D. in Chemistry from Princeton University in 1981. After a postdoctoral position at the University of Texas, Austin, he held research positions at Standard Oil of Ohio and Dupont Central Research, joining the faculty of the

Department of Chemical Engineering and Materials Science at the University of Minnesota in 1990. He moved to New York University in 2006, where he established the Molecular Design Institute and is a Silver Professor and Chair of the Department of Chemistry. Ward also is an Associate Editor for the ACS journal *Chemistry of Materials* and director of the NSF-supported NYU Materials Research Science and Engineering Center. His current research interests include organic solid-state chemistry, crystal growth, atomic force microscopy, and the role of crystallization in disease.

FOOTNOTES

*To whom correspondence should be addressed. E-mail addresses: hillmyer@umn.edu; mdw3@nyu.edu.
‖Korea Institute of Science and Technology, Seoul 136-791, Republic of Korea.

REFERENCES

1 Bernstein, J. *Polymorphism in Molecular Crystals*; Clarendon Press: Oxford, U.K., 2002.

2 Khoshkhoo, S.; Anwar, J. Crystallization of Polymorphs: The Effects of Solvent. *J. Phys. D: Appl. Phys.* **1993**, *26*, B90–B93.

3 Kitamura, M. Controlling Factors of Polymorphism in Crystallization. *J. Cryst. Growth* **2002**, *237−239*, 2205–2214.

4 Davey, R. J.; Blagden, N.; Potts, G. D.; Docherty, R. Polymorphism in Molecular Crystals: Stabilization of a Metastable Form by Conformational Mimicry. *J. Am. Chem. Soc.* **1997**, *119*, 1767–1772.

5 (a) Last, J. A.; Hooks, D. E.; Hillier, A. C.; Ward, M. D. The Physiochemical Origins of Coincident Epitaxy in Molecular Overlayers: Lattice Modeling vs Potential Energy Calculations. *J. Phys. Chem. B* **1999**, *103*, 6723–6733. (b) Price, C. P.; Grzesiak, A. L.; Matzger, A. J. Crystalline Polymorph Selection and Discovery with Polymer Heteronuclei. *J. Am. Chem. Soc.* **2005**, *127*, 5512–5517. (c) Bonafede, S. J.; Ward, M. D. Selective Nucleation and Growth of an Organic Polymorph by Ledge-Directed Epitaxy on a Molecular Crystal Substrate. *J. Am. Chem. Soc.* **1995**, *117*, 7853–7861.

6 Weissbuch, I.; Lahav, M.; Leiserowitz, L. Toward Stereochemical Control, Monitoring, and Understanding of Crystal Nucleation. *Cryst. Growth Des.* **2003**, *3*, 125–150.

7 Defay, R.; Prigogine, I. *Surface Tension and Adsoption*; Longmans: London, 1966.

8 Ha, J.-M.; Hillmyer, M. A.; Ward, M. D. Thermotropic Properties of Organic Nanocrystals Embedded in Ultrasmall Chambers. *J. Phys. Chem. B* **2005**, *109*, 1392–1399.

9 Erdemir, D.; Lee, A. Y.; Myerson, A. S. Nucleation of Crystals from Solution: Classical and Two-Step Models. *Acc. Chem. Res.* **2009**, *42*, 621–629.

10 Christenson, H. K. Confinement Effects on Freezing and Melting. *J. Phys.: Condens. Matter* **2001**, *13*, R95–R133.

11 Alcoutlabi, M.; McKenna, G. B. Effects of Confinement on Material Behavior at the Nanometer Size Scale. *J. Phys.: Condens. Matter* **2005**, *17*, R461–R524.

12 Rault, J.; Neffati, R.; Judeinstein, P. Melting of Ice in Porous Glass: Why Water and Solvents Confined in Small Pores Do Not Crystallize? *Eur. Phys. J. B* **2003**, *36*, 627–637.

13 Jackson, C. L.; McKenna, G. B. Vitrification and Crystallization of Organic Liquids Confined to Nanoscale Pores. *Chem. Mater.* **1996**, *8*, 2128–2137.

14 Olson, D. A.; Chen, L.; Hillmyer, M. A. Templating Nanoporous Polymers with Ordered Block Copolymers. *Chem. Mater.* **2008**, *20*, 869–890.

15 Zalusky, A. S.; Olayo-Valles, R.; Wolf, J. H.; Hillmyer, M. A. Ordered Nanoporous Polymers from Polystyrene−Polylactide Block Copolymers. *J. Am. Chem. Soc.* **2002**, *124*, 12761–12773.

16 Wolf, J. H.; Hillmyer, M. A. Ordered Nanoporous Poly(cyclohexylethylene). *Langmuir* **2003**, *19*, 6553–6560.

17 (a) Rzayev, J.; Hillmyer, M. A. Nanoporous Polystyrene Containing Hydrophilic Pores from an ABC Triblock Copolymer Precursor. *Macromolecules* **2005**, *38*, 3–5. (b) Rzayev, J.; Hillmyer, M. A. Nanochannel Array Plastics with Tailored Surface Chemistry. *J. Am. Chem. Soc.* **2005**, *127*, 13373–13379.

18 Ha, J.-M.; Wolf, J. H.; Hillmyer, M. A.; Ward, M. D. Polymorph Selectivity Under Nanoscopic Confinement. *J. Am. Chem. Soc.* **2004**, *126*, 3382–3383.

19 Yu, L. Polymorphism in Molecular Solids: An Extraordinary System of Red, Orange, and Yellow Crystals. *Acc. Chem. Res.* **2010**, *43*, 1257–1266.

20 Beiner, M.; Rengarajan, G. T.; Pankaj, S.; Enke, D.; Steinhart, M. Manipulating the Crystalline State of Pharmaceuticals by Nanoconfinement. *Nano Lett.* **2007**, *7*, 1381–1385.

21 Rengarajan, G. T.; Enke, D.; Beiner, M. Stabilization of the Amorphous State of Pharmaceuticals in Nanopores. *J. Mater. Chem.* **2008**, *18*, 2537–2539.

22 Rengarajan, G. T.; Enke, D.; Beiner, M. Crystallization Behavior of Acetaminophen in Nanopores. *Open Phys. Chem. J.* **2007**, *1*, 18–24.

23 Beiner, M. Nanoconfinement as a Tool to Study Early Stages of Polymer Crystallization. *J. Polym. Sci., Part B: Polym. Phys.* **2008**, *46*, 1556–1561.

24 Hamilton, B. D.; Hillmyer, M. A.; Ward, M. D. Glycine Polymorphism in Nanoscale Crystallization Chambers. *Cryst. Growth Des.* **2008**, *8*, 3368–3375.

25 Mullin, J. W. *Crystallization*; Elsevier Butterworth-Heinemann: London, 2001.

26 Ha, J.-M.; Hamilton, B. D.; Hillmyer, M. A.; Ward, M. D. Phase Behavior and Polymorphism of Organic Crystals Confined within Nanoscale Chambers. *Cryst. Growth Des.* **2009**, *9*, 4766–4777.

27 Ha, J.-M. Ph.D. Thesis, University of Minnesota. 2006.

28 Henschel, A.; Kumar, P.; Hofmann, T.; Knorr, K.; Huber, P. Preferred Orientation of n-Hexane Crystallized in Silicon Nanochannels: A Combined X-ray Diffraction and Sorption Isotherm Study. *Phys. Rev. E* **2009**, *79*, No. 032601.

29 (a) Henschel, A.; Hofmann, T.; Huber, P.; Knorr, K. Preferred Orientations and Stability of Medium Length N-Alkanes Solidified in Mesoporous Silicon. *Phys. Rev. E* **2007**, *75*, No. 021607. (b) Henschel, A.; Huber, P.; Knorr, K. Crystallization of Medium-Length 1-Alcohols in Mesoporous Silicon: An X-ray Diffraction Study. *Phys. Rev. E* **2008**, *77*, No. 042602.

30 Steinhart, M.; Stephan, S.; Wehrspohn, R. B.; Gosele, U.; Wendorff, J. H. Curvature-Directed Crystallization of Poly(vinylidene difluoride) in Nanotube Walls. *Macromolecules* **2003**, *36*, 3646–3651.

31 Hamilton, B. D.; Weissbuch, I.; Lahav, M.; Hillmyer, M. A.; Ward, M. D. Manipulating Crystal Orientation in Nanoscale Cylindrical Pores by Stereochemical Inhibition. *J. Am. Chem. Soc.* **2009**, *131*, 2588–2596.

32 Torbeev, V. Yu.; Shavit, E.; Weissbuch, I.; Leiserowitz, L.; Lahav, M. Control of Crystal Polymorphism by Tuning the Structure of Auxiliary Molecules as Nucleation Inhibitors. The *β*-Polymorph of Glycine Grown in Aqueous Solutions. *Cryst. Growth Des.* **2005**, *5*, 2190–2196.

33 Kauzmann, W. The Nature of the Glassy State and the Behavior of Liquids at Low Temperatures. *Chem. Rev.* **1948**, *43*, 219–256.

34 Debenedetti, P. G.; Stillinger, F. H. Supercooled Liquids and the Glass Transition. *Nature* **2001**, *410*, 259–267.

35 Takahashi, S.; Miura, H.; Kasai, H.; Okada, S.; Oikawa, H.; Nakanishi, H. Single-Crystal-to-Single-Crystal Transformation of Diolefin Derivatives in Nanocrystals. *J. Am. Chem. Soc.* **2002**, *124*, 10944–10945.

36 Bučar, D.-K.; MacGillivray, L. R. Preparation and Reactivity of Nanocrystalline Cocrystals Formed via Sonocrystallization. *J. Am. Chem. Soc.* **2007**, *129*, 32–33.

37 Weissbuch, I.; Leiserowitz, L.; Lahav, M. Stochastic "Mirror Symmetry Breaking" via Self-Assembly, Reactivity and Amplification of Chirality: Relevance to Abiotic Conditions. *Top. Curr. Chem.* **2005**, *259*, 123–165.